Medical Radiology · Diagnostic Imaging
Series Editors: H.-U. Kauczor · P.M. Parizel · W.C.G. Peh

Victor N. Cassar-Pullicino
A. Mark Davies *Editors*

Measurements in Musculoskeletal Radiology

Springer

Medical Radiology

Diagnostic Imaging

For further volumes:
http://www.springer.com/series/4354

VCP providing illumination while AMD attempts to restore power

Victor N. Cassar-Pullicino
A. Mark Davies
Editors

Measurements in Musculoskeletal Radiology

Springer

Editors
Victor N. Cassar-Pullicino
Department of Radiology
Robert Jones and Agnes Hunt
Orthopaedic Hospital NHS
Foundation Trust
Oswestry, UK

A. Mark Davies
Department of Radiology
Royal Orthopaedic Hospital NHS
Foundation Trust
Birmingham, UK

ISSN 0942-5373 ISSN 2197-4187 (electronic)
Medical Radiology
ISBN 978-3-540-43853-3 ISBN 978-3-540-68897-6 (eBook)
https://doi.org/10.1007/978-3-540-68897-6

Library of Congress Control Number: 2017955691

This Springer imprint is published by the registered company Springer-Verlag GmbH, DE part of Springer Nature
The registered company address is: Heidelberger Platz 3, 14197 Berlin, Germany

This book is dedicated to Wendy Pullicino

Preface

From the birth of imaging with Roentgen to the latest molecular imaging, there has always been a desire to obtain measurements that can be compared with further observation over time or with other cases. In their first edition of the *Atlas of Roentgenographic Measurement*, Lusted and Keats stated that "The interpretation of a roentgenogram remains an art ……. To this interpretation the objective evidence of the roentgenographic measurement can make an important contribution". This remains as true today as when first published almost 60 years ago. The difference now is that our knowledge of what is normal or abnormal and pathology in general has expanded almost exponentially hand-in-hand with equally dramatic advances in imaging techniques using both ionising radiation (e.g. CT and PET) and non-ionising modalities (e.g. US and MRI).

It is true to say that way back in the early 1980s, as radiologists in training, we were at best lukewarm to the concepts of measurement and their role in musculoskeletal disorders. Increasingly over the years as advances in imaging and musculoskeletal diseases have continuously evolved, we have often quoted Lord Kelvin's wise words; "To measure is to know" and "If you cannot measure it, you cannot improve it". However if a measured parameter is deemed important in science, research and clinical practice, it is imperative to realise that its value rests entirely on the adequacy, precision and accuracy of its measurement. The purpose for which the measure is intended must be clearly understood and the inferences that can be drawn need to be examined in an objective and critical manner before any conclusions are reached. All too often measurements are introduced and employed without examining their validity, which requires that rigorous steps are put in place to understand the meaning and usefulness of the measured values. The main aim of this book is to critically and clearly bring this knowledge under one roof.

As our understanding of disease processes and the sophistication of imaging techniques have improved with time, there is a need to continuously update radiologists, orthopaedic surgeons and the other allied healthcare professionals working in this field. To this end this book takes a trident approach. The first five chapters are devoted to the differing imaging techniques highlighting the strengths and weaknesses when employed to measurement. There are then 12 chapters dealing with the major anatomical areas where the relevant distilled knowledge and data are presented critically in a template format. The final four chapters are devoted to the wide range of imaging that can be applied in varied disease states.

We are particularly grateful to the international panel of authors for their expert contributions to this book, which aims to provide a comprehensive and up-to-date overview of measurements and their value in musculoskeletal radiology. The subject is diverse and complex, and the relevant publications are found scattered across multiple scientific and medical disciplines. To this end we are especially grateful to the dedicated Francis Costello Library staff at the Robert Jones and Agnes Hunt Orthopaedic Hospital, namely Marie, Fiona, Siobahn, Scott, Amanda, Karen P, Pauline, Samantha, Lis, Louisa, Karen J and Kenna, who gave every assistance and guidance in procuring the original publications. The support that we received from Springer Verlag by Ute Heilmann and her team was instrumental in seeing this book to fruition. Special thanks must also go to the immeasurable support that we received from a number of secretaries but namely Wendy and Erica. We also wish to acknowledge the endless patience, skills and unflagging fortitude of the Medical Illustration Department at the Robert Jones and Agnes Hunt Orthopaedic Hospital headed by Andrew Biggs, namely Alun, Nia, Jon and Tony, who had the task of redrawing all the figures from a variety of sources. Last and by no means least, this would not have been possible without the encouragement, patience and unselfish nature of Wendy Pullicino who was always there along the long journey—words cannot define how much we valued her support.

Oswestry, UK — Victor N. Cassar-Pullicino
Birmingham, UK — A. Mark Davies

Contents

Contributors

Christian E. Althoff Interventional Radiology Section, Charité University Hospital—Campus Mitte, Berlin, Germany

Ali Attieh Radiologia— Department of Health Science, Università di Genova, Ospedale Policlinico San Martino, Genova, Italy

Antonio Barile Department of Radiology, University of L'Aquila, L'Aquila, Italy

Andrea Baur-Melnyk Department of Clinical Radiology, University of Munich-Grosshadern, Munich, Germany

Matthias Bollow Department of Radiology, Augusta Hospital Bochum, Bochum, Germany

R. Botchu Department of Musculoskeletal Radiology, The Royal Orthopaedic Hospital, Northfield, Birmingham, UK

Nathalie Boutry Department of Musculoskeletal Radiology, Centre Hospitalier Universitaire de Lille, Hôpital Roger Salengro, CHRU de Lille, Lille Cedex, France

Victor N. Cassar-Pullicino Department of Radiology, Robert Jones and Agnes Hunt Orthopaedic Hospital NHS Foundation Trust, Oswestry, UK

Anne Cotten Department of Musculoskeletal Radiology, Centre Hospitalier Universitaire de Lille, Hôpital Roger Salengro, CHRU de Lille, Lille Cedex, France

A. Mark Davies Department of Radiology, Royal Orthopaedic Hospital NHS Foundation Trust, Birmingham, UK

Xavier Demondion Department of Musculoskeletal Radiology, Centre Hospitalier Universitaire de Lille, Hôpital Roger Salengro, CHRU de Lille, Lille Cedex, France

Department of Anatomy, Faculty of Medicine, Centre Hospitalier Universitaire de Lille, Hôpital Roger Salengro, CHRU de Lille, Lille Cedex, France

Hassan Douis University Hospital Birmingham, Birmingham B15 2TH, UK

Jean-Luc Drapé Sorbonne Paris Centre, Radiologie B, Hospital Cochin, University Paris Descartes, Paris, France

David A. Elias Department of Diagnostic Imaging, King's College Hospital, London, UK

Maria Vittoria Di Fabio Department of Radiology, University of L'Aquila, L'Aquila, Italy

J. Farrant The Royal Free Hospital, London, UK

Tobias Geith Department of Clinical Radiology, University of Munich-Grosshadern, Munich, Germany

Andrew J. Grainger Leeds Teaching Hospitals, Leeds, UK

Kay-Geert A. Hermann Musculoskeletal Radiology Section, Arthritis Imaging Research Group, Department of Radiology, Charité University Hospital—Campus Mitte, Berlin, Germany

Richard Hodgson Centre for Imaging Science, University of Manchester, Manchester, UK

Eric Hughes Department of Radiology, Robert Jones and Agnes Hunt Orthopaedic Hospital, Oswestry, UK

K. Johnson Birmingham Children's Hospital, Birmingham, UK

Anne Grethe Jurik Department of Radiology, Aarhus University Hospital, Aarhus, Denmark

Department of Clinical Medicine, Aarhus University, Aarhus, Denmark

Franz Kainberger CIR—Computational Imaging Research Lab, Department of Biomedical Imaging and Image-Guided Therapy, Medical University of Vienna, Vienna, Austria

Apostolos H. Karantanas Department of Radiology, Robert Jones and Agnes Hunt Orthopaedic Hospital, Oswestry, UK

G.M.M.J. Kerkhoffs Department of Orthopaedic Surgery, Suite G7-153, Academic Medical Center Amsterdam, Amsterdam, The Netherlands

Chadi Khalil Department of Musculoskeletal Radiology, Centre Hospitalier Universitaire de Lille, Hôpital Roger Salengro, CHRU de Lille, Lille Cedex, France

Andrea Klauser Department of Radiology, Rheuma- und Sportbildgebung, Medical University Innsbruck, Innsbruck, Austria

Georg Langs CIR—Computational Imaging Research Lab, Department of Biomedical Imaging and Image-Guided Therapy, Medical University of Vienna, Vienna, Austria

Thomas M. Link Department of Radiology and Biomedical Imaging, University of California, San Francisco, San Francisco, CA, USA

Eva Llopis Hospital Universitario de la Ribera, Alzira, Valencia, Spain

M. Maas Department of Radiology, Suite G1-211, Academic Medical Center, Amsterdam, The Netherlands

Fabio Martino Department of Radiology, ASL BARI, Bari, Italy

Gianluigi Martino Radiology Department of the P.O., "Di Venere" - ASL BARI, Bari, Italy

Carlo Martinoli Radiologia— Department of Health Science, Università di Genova, Ospedale Policlinico San Martino, Genova, Italy

C. Miller Birmingham Children's Hospital, Birmingham, UK

S. Mohan Birmingham Children's Hospital, Birmingham, UK

C.M. Nusman Department of Radiology, Suite G1-211, Academic Medical Center, Amsterdam, The Netherlands

Philip James O'Connor Leeds Teaching Hospitals Trust, The University of Leeds, Leeds, UK

Mario Padrón Clinica Cemtro, Madrid, Spain

Philipp Peloschek Radiology Centre Vienna, Vienna, Austria

R.R. van Rijn Department of Radiology, Suite C2-423.1, Academic Medical Center Amsterdam, Amsterdam, The Netherlands

Andrew Roberts Children's Unit Robert Jones and Agnes Hunt Orthopaedic Hospital, Oswestry, UK

Clare Roche Department of Radiology, University College Hospital Galway (UCHG), Galway, Republic of Ireland

Eugenie Sánchez Clinica Cemtro, Madrid, Spain

Jaspreet Singh Department of Radiology, Robert Jones & Agnes Hunt Orthopaedic Hospital, Oswestry, UK

Michele Solarino University of Bari, Bari, Italy

P.A.A. Struijs Department of Orthopaedic Surgery, Suite G7-152, Academic Medical Center Amsterdam, Amsterdam, The Netherlands

Alberto Tagliafico Radiologia— Department of Health Science, Università di Genova, Ospedale Policlinico San Martino, Genova, Italy

Nicolas Theumann Department of Radiology, Clinique Bois-Cerf, Lausanne, Switzerland

Prudencia N.M. Tyrrell Department of Radiology, Robert Jones & Agnes Hunt Orthopaedic Hospital, Oswestry, UK

Filip M. Vanhoenacker Department of Radiology, University Hospital Antwerp, Antwerp University, Edegem, Belgium

Department of Radiology, AZ Sint-Maarten, Duffel-Mechelen, Duffel, Belgium

Department of Radiology, University Hospital Ghent, Ghent, Belgium

Koenraad L. Verstraete Department of Radiology, University Hospital Ghent, Ghent, Belgium

Reinhard Windhager Department of Orthopaedic & Trauma Surgery, Medical University of Vienna, Vienna, Austria

Richard W. Whitehouse Department of Clinical Radiology, Manchester Royal Infirmary, Manchester, UK

Naomi Winn Department of Radiology, Robert Jones and Agnes Hunt Orthopaedic Hospital NHS Foundation Trust, Oswestry, UK

Part I

Measurement Techniques

The Radiograph

1

Eric Hughes, Prudencia N. M. Tyrrell,
and Victor N. Cassar-Pullicino

Contents

1.1 Introduction

Radiographs have been used in diagnosis for over 100 years. Despite the many technical advances in imaging, they retain an important role in the diagnostic workup of many ailments particularly in bone and joint pathology. They are often used in imaging follow-up of disease states to evaluate progression, monitor treatment or assess metalwork or implants following surgery. It is possible from the radiographs to make measurements which aid in diagnosis or subsequent management of a condition. Sometimes, these measurements are crude representing an observation such as the presence of prevertebral soft tissue swelling in a patient with a history of cervical spine injury where that observation signals a very high probability of either bone or soft tissue injury. On other occasions, precise measurements may be required such as in leg length evaluation which may determine the degree and extent of surgical intervention if indeed any. They also are often used for measuring distances and angles in musculoskeletal work to assist in the planning of management including surgery. There are inherent advantages in using radiographs for such measurements, but there are also certain limitations often related to technical factors of which clinicians and radiologists need to be aware. This chapter addresses the general role of radiography in measurements undertaken in musculoskeletal work. The specific role of radiography in measurements of different anatomical and pathological states is made in the relevant chapters.

E. Hughes, H.D.C.R. (✉) • P. N. M. Tyrrell, M.D.
V. N. Cassar-Pullicino, M.D.
Department of Radiology, Robert Jones and Agnes Hunt Orthopaedic Hospital NHS Foundation Trust, Oswestry, UK
e-mail: eric.hughes@rjah.nhs.uk

V. N. Cassar-Pullicino, A. M. Davies (eds.), *Measurements in Musculoskeletal Radiology*,
Medical Radiology, Diagnostic Imaging, https://doi.org/10.1007/978-3-540-68897-6_1

1.2 Advantages of Radiographs

Radiographs are cheap and readily available. Standardisation of the radiograph is possible such that they can be directly compared both within a department and between different departments. Thus, they are reproducible and in this context can be used in research. The conventional radiograph can be used to monitor progress of a condition such as rheumatoid arthritis by documenting joint space narrowing and number of erosions. It can be used to monitor healing of bone injury documenting new bone formation and progressive consolidation or otherwise. It can be used to monitor the effect of therapy or response to treatment such as may be seen with effective antibiotic treatment in osteomyelitis or appropriate biochemical or endocrine treatment in osteomalacia. Serial lateral radiographs of the thoracic and lumbar spine are used in the monitoring of osteoporosis. Grading systems have developed and employed radiographic appearances to denote severity of disease which is used in therapeutic decision making, e.g. trauma and avascular necrosis. The earliest changes of disease processes, however, may not be seen on radiographs, such as avascular necrosis, and other imaging modalities such as magnetic resonance imaging may need to be employed. Once the radiographic features are detectable, then the radiograph may be used for disease monitoring in some instances. Many surgical instrumentation procedures are monitored over time with periodic radiographs. This is perhaps most commonly seen in patients who are being followed up post arthroplasty. Monitoring of disease with serial or sequential radiographs provides objective evidence as a guide to decision-making for operative or nonoperative treatment. In the examples given above, eyeballing the radiograph to assess status can be adequate. However, there will be many instances where accurate measurements are required in order to determine planning of corrective surgery, for example, in children with unequal leg lengths. Accurate measurements are also required to facilitate evidence-based studies. This can be seen in patients with spinal infection where the disc has been destroyed with associated loss of vertebral body height. Should vertebral body collapse with kyphotic deformity progress to a particular level, then surgery with instrumentation may be necessary to stabilise the spine and prevent further deformity. Such objective evidence with measurement of the degree of angulation facilitates evidence-based outcomes of treatment.

Assessment of bone age and potential for growth in the immature skeleton is important in treatment planning. This can be done using a number of indices. The Greulich and Pyle atlas of hand radiographs (Greulich and Pyle 1959), or the Sauvegrain method of bone age estimation on elbow radiographs (Sauvegrain et al. 1962) between the approximate ages of 11 and 16 years, are just two of a number of methods available. All methods of estimating skeletal age involve comparing radiographs of the patient with standards in an atlas. This estimation is only moderately accurate. In the Tanner and Whitehouse method (Tanner et al. 1975), 20 indicators on hand and wrist radiographs are assessed and given a score, yielding a total score from 0 to 100. The Risser sign relates to the degree of ossification of the iliac apophysis (Risser 1958). This is a commonly used marker of skeletal maturation especially in the treatment of scoliosis. A bone age estimation in isolation is meaningless. The measurement needs to be compared with the chronological age and ideally the rate of annual growth in standing height assessed.

One particular advantage of plain radiographs, not readily available with other imaging modalities, is the facility to obtain dynamic views in, for example, flexion and extension. This allows a rapid evaluation of stability. Abnormal movement can be detected by eyeballing the radiograph or discrete measurements can be obtained if necessary. Stress views, e.g. at the knee or ankle, can be used for the evaluation of ligamentous integrity.

Radiographs are good for providing both an informal and formal assessment of measurement, but there are a number of technical issues which need special consideration when highly accurate measurements are required. These are addressed in detail below.

1.3 Limitation of Radiographs for Measurement

Despite the many advantages of radiographs for use as a measuring tool in orthopaedic and musculoskeletal work, there are a number of limitations. To understand the nature of these limitations and how they may be overcome, it is helpful to reflect on how X-rays are produced. Although many departments are now using some form of digital radiography, basic principles of both film and digital imaging are covered. In line with commonly used terminology, this text refers to focus film or object film distances, and use of the term film in this instance can refer to a film cassette, computerised radiography plate or a direct digital radiography detector plate.

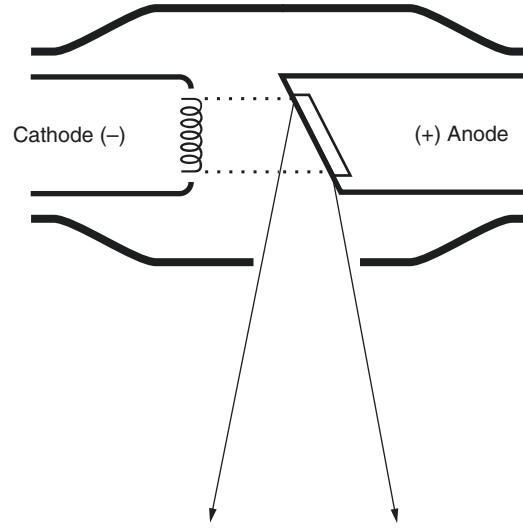

Fig. 1.1 X-ray tube simplified representation

Basic Principles of X-ray Production

A focused beam of electrons is accelerated between the cathode and anode of an X-ray tube striking the anode at high speed within a small area to produce what is as close to a point source of X-rays as is possible within the efficiency limitations of the system (Fig. 1.1).

The resultant X-rays are emitted in all directions but are contained within the housing of the X-ray tube with the exception of a small window which, with the addition of adjustable lead slats, can result in a directed divergent adjustable beam of X-ray. The portion of the beam which is passed through the object without being deflected forms the shadow image on a film or an image receptor plate. Scattered radiation reaches the film in a random way and does not contribute to the useful image. This scattered radiation may need to be reduced by the use of a lead-slatted grid.

In order to reduce the amount of radiation required to form the image and reduce the radiation dose to the patient, the use of film has been supplemented by the use of intensifying screens which convert each X-ray photon into several light photons. It is therefore the light emitted by the intensifying screens which forms the majority of the image on the film. Conventional film screen cassettes produce an analogue image recorded on film and developed using a photographic process. These are viewed on a lightbox. All the information is in the hardcopy image only and the image cannot be manipulated. Within PACS digital systems, a similar effect is generated by the use of mathematical algorithms. In the technique of computed radiography (CR), a photostimulable phosphor contained within a cassette is exposed in the same way as conventional film and then removed to be read remotely by a laser mechanism. Direct digital radiography (DDR) uses solid-state detectors to record the latent image, but this is linked directly to the readout device, therefore requiring much higher costs for replacing the X-ray imaging hardware. Digital radiographs, whether produced by CR or DDR, can be manipulated, contrast enhanced and edges sharpened, and with appropriate software, measurements can be readily obtained.

MRI, CT and nuclear medicine are digital imaging techniques where the information contained in the image is stored in numerical form and thus can be manipulated in order to enhance contrast resolution. Spatial resolution can also be controlled by altering pre-imaging parameters. This technological advancement has been slower in conventional radiography, and there are at present a number of options for recording and thus measuring from the radiographic image.

1.4 Technical Limitations of Radiographs for Measurement

These fall into three categories:

1. Resolution—contrast and spatial
2. Magnification
3. Distortion

Resolution: Contrast and Spatial

The resolving capability of a particular radiographic material or fluorescent screen image is a measurement of the degree of fine detail which can be recorded. It is related to the unsharpness characteristics of the material as it is a measure of the ability to differentiate between adjacent positional detail. Resolution is often expressed as the number of lines per millimetre that can be seen as separate elements of an image. Spatial resolution is high for detailed conventional radiography as compared to CT where the degree of spatial resolution is limited by the field of view and matrix size employed.

The attenuation of the X-ray beam is inversely proportional to the square of the atomic number of the object/tissue being imaged. Therefore, the higher the atomic number, e.g. cortical bone, the greater will be the attenuation of the X-ray beam, and the lower the atomic number, the less the beam is attenuated as it passes through the tissue. In conventional radiography, tissues with a wide difference in density, such as cortical bone and soft tissue, can be readily appreciated. Tissues with a narrower difference in density such as fat and muscle can be differentiated but will require optimum viewing conditions to appreciate. Tissues with potentially a very narrow difference in density such as muscle and a non-metallic foreign body such as glass will require close attention by the radiographer to exposure factors (kilovoltage (kVp) and milliampere seconds (mAs)) and optimum viewing conditions for the reporting radiologist. The kilovoltage used is a major determinant of contrast resolution. In conventional radiography, contrast can be altered by adjustment of exposure parameters and is very much less than that which can be achieved with computed axial tomography (CT). Radiography is excellent for the evaluation of bone detail, whereas the soft tissue detail is poor. A large knee joint effusion is seen as distension of the suprapatellar pouch, but it can be extremely difficult if not impossible to identify if the joint distension is due to serous fluid from an arthritic process, due to pus from an infected joint or due to blood following trauma. If a haemarthrosis occurs in association with a fracture, then a fluid-fluid level due to layering of different density materials may be identified on a horizontal shoot-through radiograph.

Contrast and image sharpness have both subjective and objective connotations. Subject contrast is mainly influenced by kilovoltage and scattered radiation. The degree of scatter can be reduced by the use of grids.

Image sharpness is affected by the geometry of the equipment including the size of the focal spot and the relative distance between the focal spot, the subject and the film. The degree of geometric unsharpness can be controlled in several ways:

1. By using a smaller focal spot.
2. By decreasing the object to film distance.
3. By increasing the focus to object distance. In practice, this is equivalent to increasing the focus to film distance.

Focus Size

The production of X-rays is an inefficient system with approximately 98% of the energy used being produced as heat. With temperatures of the tube anode reaching close to 3000 °C during exposure, there is a need to dissipate heat effectively from the anode. This is achieved by use of a rotating angled anode and the ability of the operator to select one of two electron distribution areas on the anode referred to as the broad or the fine focus. Modern imaging units have an effective fine focus of the order of 0.4–0.6 mms and a broad focus of the order of 1.0–1.5 mms. The use

of an X-ray source of a finite size leads to penumbra effect which diffuses the edge of an object rendering it less distinct than if a point source was used (Fig. 1.2). At an operational focus to film distance of 100 cm or more, the effective width of the penumbra is minimal, but the smaller the value of the focus to film distance, the greater the penumbra effect.

Another cause of slight unsharpness of an object image when using film is the parallax effect. Radiographic film is made up of two separate emulsion coatings separated by a film base. X-irradiation or light striking the film will form two images. These can only be directly superimposed when viewed at the same angle as that at which the image forming radiation fell onto the film. Any slight offset between the two images is known as the parallax effect. Movement of the patient during the exposure and also the duration of the exposure itself may contribute to slight variations in image sharpness.

The use of intensifying screens can also be used to improve detail of the image. An intensifying screen consists of crystals suspended within a binding material. Faster screens which require a reduced number of photons to form the image have larger crystals which emit light when struck by an X-ray photon. The larger crystals limit the ability of the resultant image to resolve smaller structures. Slower intensifying screens which are designed to provide high detail have smaller crystals and a dye within the screen to limit the diffusion of light within the binder. This enables such a system to resolve between smaller structures.

For CR or DDR systems, the resolution of the system is dependent on the physical limitations of the plate reader (CR) or the photostimulable material used (DDR) to collect the image. Generally, digital systems are inferior to film in resolution, but this reduction in image quality is overridden by the flexibility offered by PACS software systems.

Some radiographic measurements are dependent on both spatial and contrast resolution. Exposure factors are very important here, and this is particularly in relation to measurements such as cortical thickness, joint space, size of erosions and prosthetic-bone-cement interfaces.

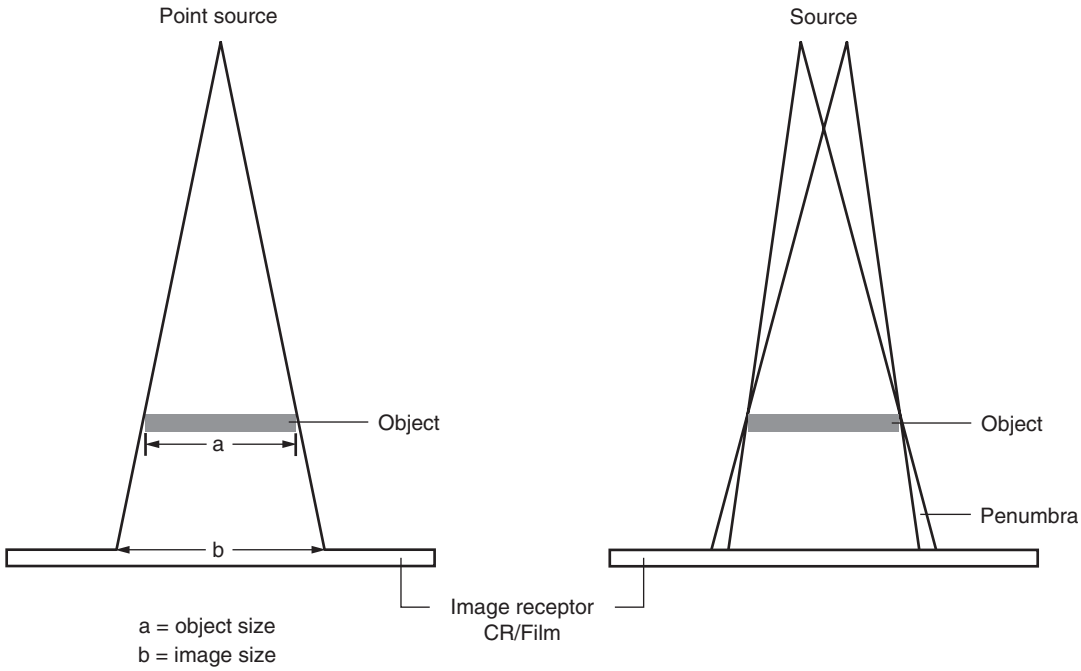

Fig. 1.2 Penumbral effects (see text)

Distortion

Image distortion results from the oblique projection of the image and can be produced in one of two ways:

1. Radiography using an angled beam (Fig. 1.3)
2. Radiography of an object not parallel to the film (Fig. 1.4)

Such image distortion can interfere with measurement, for example, in evaluation of the joint space where there may be a degree of flexion (deformity or positional). In a routine radiograph of the knee joint, the tibial condylar region slopes downwards by approximately 15° posteriorly, and therefore, in the standard anteroposterior view of the knee joint, the tibial plateau is not seen tangentially. Tibial plateau/condylar fractures can be overlooked on this account. An AP projection with 15° caudal angulation produces a tangential view of the plateau and facilitates observation of depressed fractures. Objects can also be angled in relation to the film in more than one plane and can therefore be distorted in more than one plane, e.g. scoliosis and kyphosis.

Magnification

The X-ray beam diverges from the focus of the X-ray tube in straight lines so that the cross-sectional area of the beam increases with increasing distance from the X-ray source (Fig. 1.5). Therefore, the radiographic shadow image is always larger than the original subject and hence subject to a degree of magnification. The degree of magnification is calculated by the focus to film distance divided by the focus to object distance. The actual size can then be calculated:

Actual size = image size/magnification.

Within an imaging department, there are factors which will affect magnification:

1. Different manufacturer equipment and models will have different tabletop to film distance.

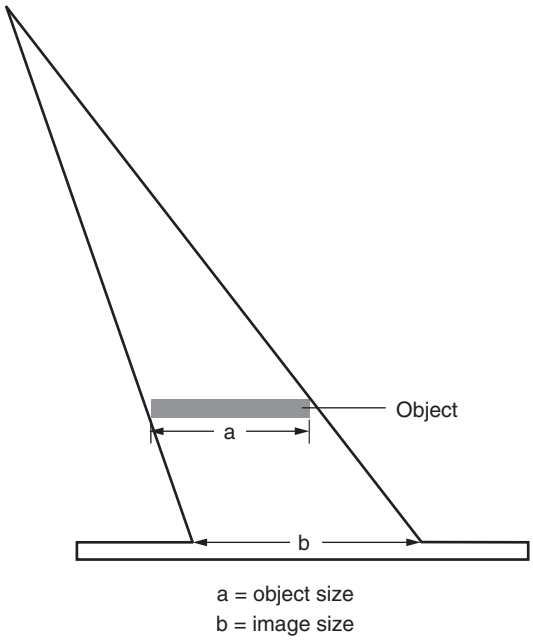

Fig. 1.3 Distortion, angled beam (see text)

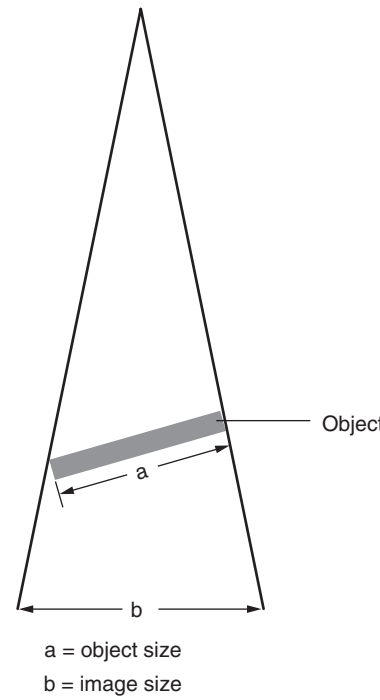

Fig. 1.4 Distortion, object not parallel to the film (see text)

This will contribute to the total object to film distance.
2. Physical size of the patient.
3. Departmental standard focus to film distance and the radiographer adherence to the standard. It must not be assumed that the presence of a standard guarantees that each image will be undertaken at the correct distance. It will vary between X-ray rooms in the same department.

Measurements taken direct from a radiograph are always subject to a degree of magnification. Even with radiography where the object imaged is in direct contact with the film, for example, weight-bearing views of the feet, there will always be a degree of magnification involved because the object imaged always has some thickness. The user must be aware that if taking a measurement from an uncalibrated image, they will not know the extent of magnification to which the object has been subjected. Many methods exist to calibrate an image. The favoured method is using a spherical object (as this is not subject to projectional distortion) of a known size placed at the same object to film distance as the object to be measured, e.g. in planning prosthetic requirement. The magnification to which the calibrating sphere has been subjected is calculated by magnification equalling measured size divided by actual size. In certain situations where direct measurements are required, such as for leg lengths, a measuring ruler can be placed beside the patient and radiographed beside the leg such that any magnification incurred will relate to both the image structure and the ruler measure facilitating a more accurate measurement. For PACS systems, plate (and therefore pixel size) is known and it may appear that there is increased accuracy in using measurement systems inbuilt within the PACS software. These systems however are not calibrated and some assume a magnification factor in the order of 10%. PACS imaging is subject to the same physical factors which affect radiographic film imaging.

Accurate measurements of joint space can be very important when trying to measure rate of disease progression in arthritis and particularly when this is part of a trial to evaluate the effect of disease modifying drugs in arthritis. The use of the semi-flexed anteroposterior view, using a horizontal X-ray beam to produce a beam tangential to the tibial plateau and using fluoroscopy to achieve reproducible alignment, has been valuable (Buckland-Wright 1995). Microfocal radiography has been shown to improve reproducibility of joint space width measurement compared to standard radiography. The chief advantage of microfocal radiography is its spatial resolution, of the order of 10–100 μm, as compared to 300–1000 μm for standard radiography. The first longitudinal study of rates of joint space narrowing measured using microfocal radiography was carried out by Ward and Buckland-Wright (2008) which showed a lowered variability of the rate of joint space narrowing but the high cost and low availability of microfocal equipment remains a barrier to its more widespread use.

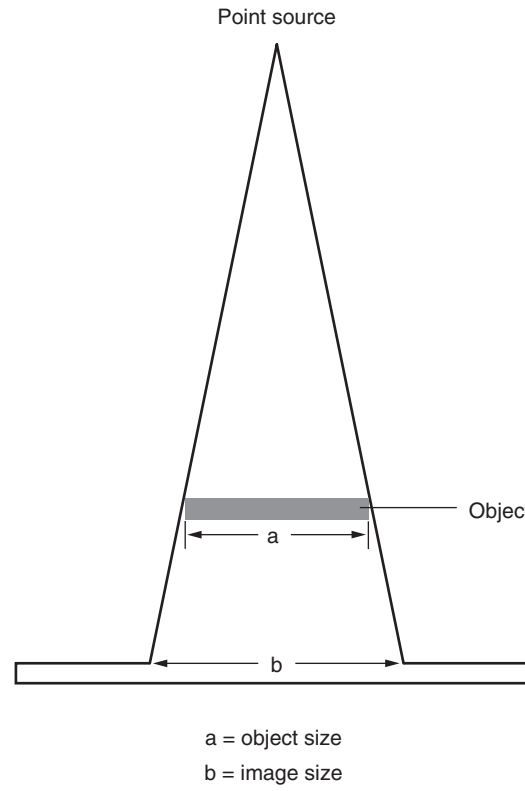

Fig. 1.5 Magnification effects (see text)

1.5 Anatomical Determinants

Anatomical features in certain areas of the body are associated with difficulties in obtaining accurate radiographic assessment and measurement. Such areas include:

1. The patellofemoral joint. Knee flexion to varying degrees has been advocated for the assessment of patellofemoral joint alignment. The conventional radiographic technique of a skyline view in 45° flexion with the X-ray beam angled 30° towards the floor (Merchant's view) (Merchant et al. 1974) has been largely superseded by CT or MR assessment in varying degrees of flexion (10–30°), as at 45° the patella is forced into the intercondylar notch even when prone to subluxation or maltracking (Walker et al. 1993).
2. The hip joint when evaluating for SUFE. An X-ray image is a two-dimensional view of a three-dimensional object. By taking two views at right angles to each other, a three-dimensional image can be built up visually. However, the axial or Z projection is not obtainable, and thus, measurements that might be valuable in this plane cannot be obtained. The angle of slip in SUFE is well seen on axial CT or MR images.
3. Weight-bearing views. These are more accurate for the depiction of joint space narrowing especially in arthritic states. It is important that when comparative assessments are made that like is compared with like, i.e. weight bearing with weight bearing.
4. Dynamic views. A linear measurement in orthopaedics is taken between two bone points of interest. At rest, this measurement can be within the normal range implying that the stabilising soft tissue structures are intact. Dynamic views unmask the loss of soft tissue integrity by showing differing measurement between the same bone points which lies outside the normal range, as may be found, for example, following a spinal injury, or in cases of instability arising in other conditions such as rheumatoid arthritis (Fig. 1.6).

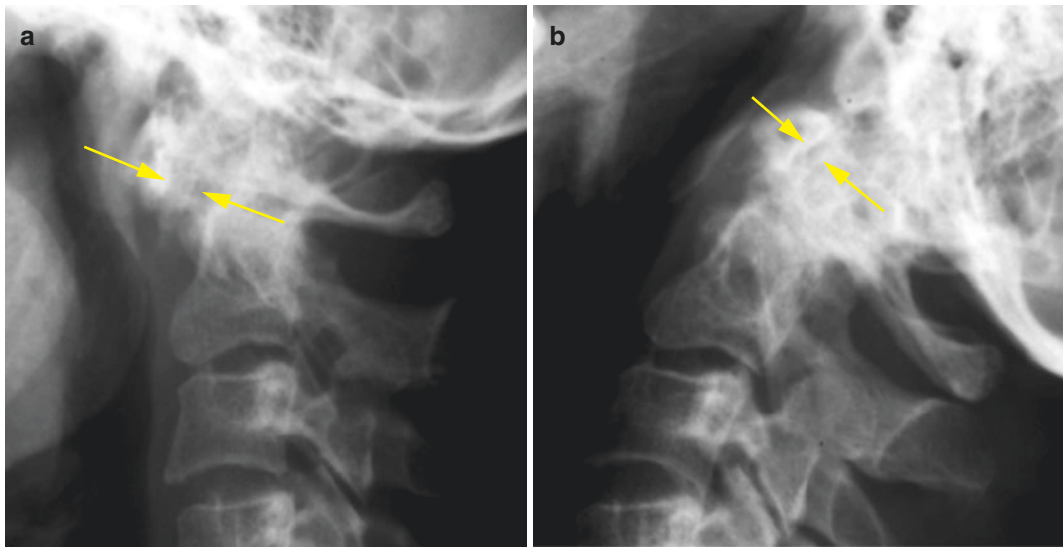

Fig. 1.6 (**a**, **b**) Lateral radiographs of the cervical spine in (**a**) flexion and (**b**) extension in a patient with rheumatoid arthritis. Note the abnormal movement at the atlanto-axial junction (arrows), with marked widening in flexion indicating anterior atlanto-axial instability

1.6 Orthopaedic Templating

Orthopaedic templating is an important element of pre-surgical planning for arthroplasty surgery where the appropriate size of implant to be used must be determined prior to surgery.

This has traditionally been undertaken using acetate templates provided by implant companies which were placed over conventional X-ray images. The acetates enabled the selection of the appropriate-sized implant with measurements in theatre contributing to the final choice of implant. These acetates assume a standard magnification for all radiographs of a particular joint, e.g. 10% for hip images.

With the advent of PACS, the overlay of an acetate template is no longer possible. A number of commercial software packages have been developed which will work within or separate to PACS enabling the user to assess the size of implant required. For accuracy, the magnification of the image must be calculated. This can either be by assessing the magnification of an object of a known size (e.g. a metallic ball) or by calculating the magnification by measurement of the focus to film distance and the object to film distance.

For the use of an object of a known size, accurate calibration relies on the placement of the object at the same distance from the film as the anatomical feature to be measured, in this case the head of femur. Such systems are therefore reliant on the careful placement of the calibrating object.

There is evidence to suggest (Franken et al. 2010) that more accuracy can be gained by measurement of the focus to film and object to film distances and calculating the magnification in this way. This can be achieved using callipers or commercially available products.

Some PACS systems will make an assumption in relation to magnification if no calibration is supplied, and care must be taken to ensure that where accurate measurement is required, e.g. the provision of custom implants, these are only taken using calibrated images.

Many companies are now developing the functionality of the software packages beyond orthopaedic templating to enable the determination of angles and the ability to aid surgical planning by estimating the appropriate size required for:

1. Plates
2. Nails
3. Screws

Many packages now offer the ability to determine osteotomy planning and specific paediatric planning and may prove to be more reliable than conventional methodology (Hankemeier et al. 2006).

Where CT images are available, orthopaedic templating is also available using 3D information. It is anticipated that the use of such software packages will grow in direct relation to the increasing use of PACS systems.

1.7 The Role of the Radiograph Related to Other Imaging Techniques

As outlined earlier in this chapter, radiographs have many advantages as a technique for measurement of various parameters in musculoskeletal conditions. There are limitations however which are largely related to contrast (largely related to the soft tissues) and also to image sharpness which can lead to blurring of image margins and hence a reduction in accuracy of the measurement. The advantages of other specific imaging modalities will be addressed in later chapters. Ultrasound is particularly good for superficial soft tissue measurements. CT with its superb contrast resolution particularly cross-sectional assessment of bone structures facilitates measurement in all imaging planes including the Z projection. MR with its particular soft tissue contrast allows evaluation of both soft tissue and marrow measurements again in all three imaging planes and indeed also in oblique planes as required. Conventional radiography however is readily available in most departments, is universal and can be reproduced at minimal relative cost. This ensures that it will remain as a mainstay in both diagnostic and evaluation processes for some time. However, even with the advent of PACS, care must be taken as regards calibration and ensuring accuracy of measurement techniques.

References

Buckland-Wright C (1995) Protocols for precise radio anatomical positioning of the tibiofemoral and patellofemoral compartments of the knee. Osteoarthr Cartil 3(Suppl A):71–80

Franken M, Grimm B, Heyligers I (2010) A comparison of four systems for calibration when templating for total hip replacement with digital radiography. J Bone Joint Surg (Br) 92-B:136–141

Greulich W, Pyle S (1959) Radiographic atlas of the skeletal development of the hand and wrist. Stanford University Press, Stanford, CA

Hankemeier S, Gosling T, Richter M, Hufner T, Hochhausen C, Krettek C (2006) Computer-assisted analysis of lower limb geometry: higher intraobserver reliability compared to conventional method. Comput Aided Surg 11(2):81–86

Merchant AC, Mercer RL, Jacobsen RH, Cool CR (1974) Roentgenographic analysis of patellofemoral congruence. J Bone Joint Surg Am 56:1391–1396

Risser JC (1958) The iliac apophysis: an invaluable sign in the management of scoliosis. Clin Orthop 11:111

Sauvegrain J, Nahm H, Bronstein N (1962) Etude de la maturation asseuse du coude. Ann Radiol 5:542

Tanner J, Whitehouse R, Marshall W et al (1975) Assessment of skeletal maturity and prediction of adult height (TW2 method). Academic, London

Walker C, Cassar-Pullicino VN, Vaisha R, McCall IW (1993) The patello-femoral joint—a critical appraisal of its geometric assessment utilising conventional axial radiography and computed arthrotomography. Br J Radiol 66(789):755–761

Ward RJ, Buckland-Wright JC (2008) Rates of medial tibiofemoral joint space narrowing in osteoarthritis studies consistent despite methodological differences. Osteoarthr Cartil 16(3):330–336

Computed Tomography

2

Richard W. Whitehouse

Contents

R. W. Whitehouse
Department of Clinical Radiology,
Manchester Royal Infirmary,
Oxford Road, Manchester M13 9WL, UK
e-mail: richard.whitehouse@cmmc.nhs.uk

2.1 Introduction

Measurements relevant to the musculoskeletal system that can be made on CT include distances and angles from the scout view, distances, angles and CT numbers from individual axial sections and more complex three-dimensional distances and angles from separate axial sections or reformatted images. Volumes can be estimated from the measured dimensions of the tissue in question or by summing the product of cross-sectional area measurements and slice spacing. CT number measurement gives rise to tissue density estimation, the accuracy of which can be improved by dual-energy scan techniques.

The use of computed tomography for distance and angle measurements has both advantages and limitations compared with plain film radiography, ultrasound and magnetic resonance imaging. Because X-rays travel in straight lines, the location of points defined by axial CT images should not be distorted in the *X* or *Y* directions, unlike MR images where image distortion by magnetic field variations occurs. The geometric magnification that occurs in conventional radiography does affect the CT scout view, as described below. Point location in the *Y*-axis (along the direction of table travel) may be less accurate on axial images, due to the slice thickness, but multislice spiral scanners are

V. N. Cassar-Pullicino, A. M. Davies (eds.), *Measurements in Musculoskeletal Radiology*,
Medical Radiology, Diagnostic Imaging, https://doi.org/10.1007/978-3-540-68897-6_2

capable of isometric (*X*, *Y* and *Z* plane) resolution so that measurements between points located on different axial slices should be of comparable accuracy to in-plane measurement. CT utilises ionising radiation, the minimum number of axial sections and lowest mA and kV settings that can produce acceptable images should routinely be used.

There is little recent literature confirming the in vitro accuracy of CT length and angle measurements, with most of the early studies published in the German literature. This chapter is therefore illustrated with in vitro scans depicting measurements that have been compared with the results of calliper and protractor measurements of the scanned objects.

2.2 Scout View Measurements

The scout view is generated by smooth, uniform velocity movement of the scanner table through the scanner aperture, whilst a thinly collimated fan beam of X-rays from the stationary tube is projected across the aperture to the detectors. The data acquired from the detectors at each point in time forms one line across the final image, the location of which within the image is directly related to the table location at that point in time. Consequently, measurements along the long axis of the scanner are potentially as accurate as the table location, which is calibrated to an error of less than 0.5 mm. Measurement across the image is, however, distorted by the fan beam geometry, with objects closer to the X-ray tube being magnified in this direction relative to those nearer the detectors. The image is calibrated to give accurate measurement across the image at the gantry isocentre; consequently table height adjustment to bring the structure being measured as close to the isocentre as possible is necessary for the most accurate result. Figure 2.1 illustrates the effect of altering table height on scout view measurements, using a femur as a test object. Small metallic markers were placed on the top of the femoral head, on the top of the femoral neck, on the lesser trochanter and on the back of each femoral condyle. These can be seen in Fig. 2.1a. Figure 2.1b–d shows the scout view appearances with the table as low as possible (closest to the

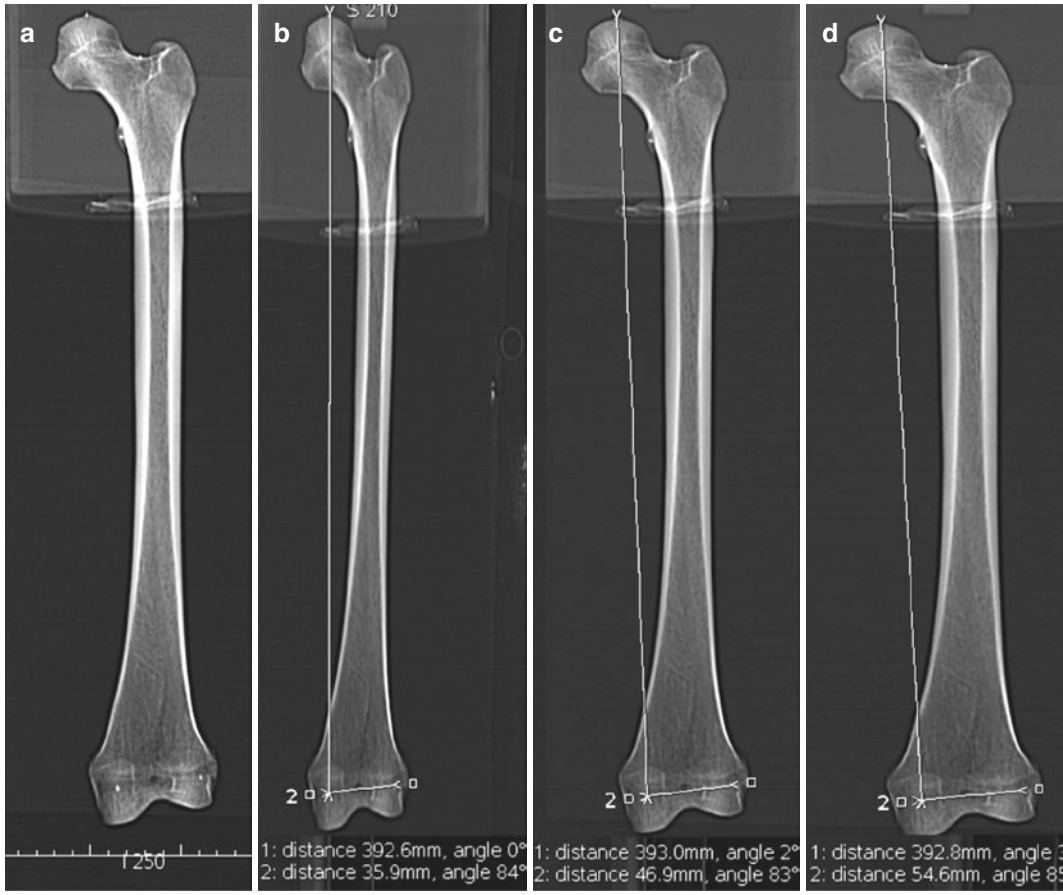

Fig. 2.1 Scout view (scan projection radiographs) of a dry femur at various table heights, demonstrating distortion across the image by geometric magnification. (**a**) With the femur at the isocentre. Note small metal markers are present on the head, neck and condyles for measurements. The apparent length of the bone is not altered in any of the subsequent views. (**b**) Table at its lowest setting. (**c**) Table adjusted to put the femur at the isocentre. The apparent width between the condyle markers is the same as that measured on the specimen. (**d**) Table at its highest setting. The apparent width of the bone is increased

detectors), at the isocentre, and as high as possible (close to the tube). The length of the femur, between the top of the head and the marker on the medial femoral condyle, is not significantly different between these scans, and results of 392.6, 393 and 392.8 mm are all within a reasonable measurement error of the 392 mm distance measured with callipers on the femur. The measurement between the condyle markers varies from 35.9, through 46.9 to 54.6 mm with the different table heights, compared with a calliper measurement of 47 mm, confirming the accuracy of measurement at the isocentre but showing errors of −23% to +16% at the other positions. Angles measured from scout views will have composite errors, from distortion by magnification across the image and also a projection error if the points being measured represent structures at different heights from the tabletop (i.e. if the plane of the measurement points is not perpendicular to the centre of the fan-beam).

Scout views are equivalent to digital radiography, using highly efficient solid-state X-ray detectors on modern multislice scanners. Consequently, a satisfactory image can be achieved at lower radiation doses than required for conventional radiography. When used for lower limb length measurement, further effective dose reduction can be achieved with the use of gonad protection.

2.3 Axial Plane Measurements

On a single axial CT image, distance and angle measurements are standard scanner console or workstation functions. As Fig. 2.2 demonstrates, angles measured from a scanned protractor are within 1° of the expected measurement. Similarly, distances are within 1 mm of the expected distance as measured on the scanned set square. The precisions of such measurements are dependent upon the reproducibility of the placement of measurement points. The scanned image is accurate to the resolution of the scanner (two to three line pairs per millimetre on a small field of view), but the reproducibility of placement of points from which measurements might be taken will be influenced by partial volume averaging, mislocation of the slice and inter- and intra-operator variations.

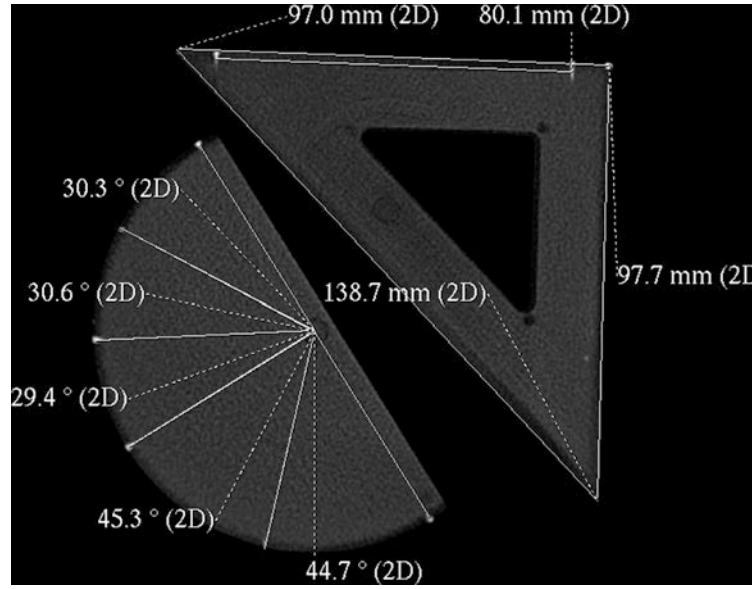

Fig. 2.2 CT scan of a plastic protractor and a set square. Radiodense markers were placed at fixed points on these objects and measurements between them made on the scanner workstation. All distances were within 0.5 mm and angles within 0.7° of expected

2.4 Three-Dimensional Measurements

When measuring between points on different sections, three-dimensional geometrical calculations are required. If a complete dataset is acquired, with all sections between the two measurement points being available, then a reformatted image on the workstation, angled to include both points, can be used to make the measurement, using the workstation software (Fig. 2.3). If only selected sections are performed (to reduce X-ray exposure to the patient), then the locations in space for each point can be identified as *X*, *Y* and *Z* Cartesian coordinates, from which the distance between the points can be calculated (a visual representation of this is shown in Fig. 2.4). Similar calculations can be derived for angle measurements between points on separate slices. When applied to a dry skull, linear distances between fixed points, measured as coordinates, were accurate to within 5% when slice thicknesses of 3 mm or less were used but exceeded this error for thicker sections (Togashi et al. 2002).

Measurement of the bone torsion usually relies on measuring planes through defined points at each end of the bone and then calculating the angle between the two planes. A plane is defined by three points in space, but only two points are used for each plane in these estimations, as the plane is assumed to be parallel to the *Z*-axis of the image dataset. This assumption is only valid if

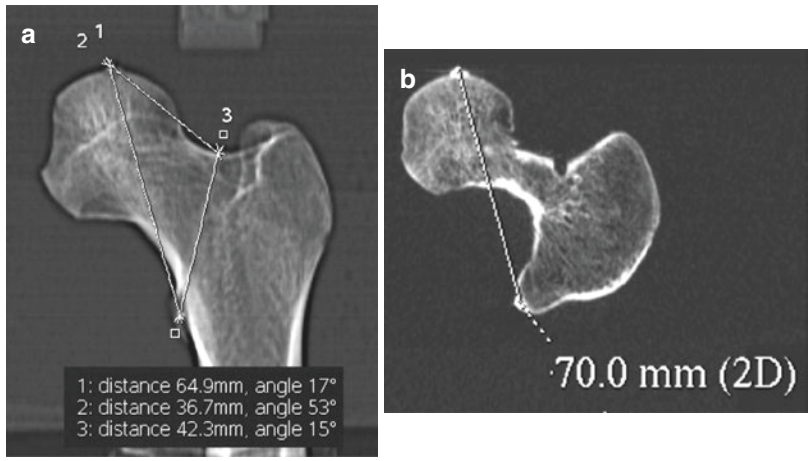

Fig. 2.3 (**a**) Scout view of the upper femur, at the isocentre. The measurement number 1 is between the metal markers on the top of the femoral head and the lesser trochanter, estimated at 64.9 mm on the scout view. These markers were not in the same plane relative to the tabletop; consequently, this distance is foreshortened on the scout view. (**b**) Coronal oblique reconstruction from axial 0.6-mm-thick contiguous sections to pass through both the metal markers described in (**a**). The distance between them now measures 70 mm, identical to that measured with callipers on the specimen

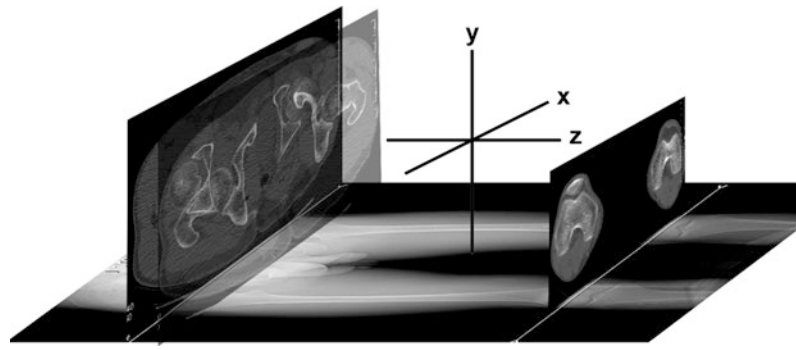

Fig. 2.4 Composite image demonstrating the relationship between sections containing measurement points, the scout view and the *X*, *Y* and *Z* axes of the dataset

the long axis of the bone being measured is aligned along the *Z*-axis (direction of table travel). The two points defining each plane may not be on the same axial section. Consequently, superimposition of the axial images (Fig. 2.5) (or transfer of the *x*,*y* coordinates of one point to the image containing the second point (Fig. 2.6)) is used to measure the angle between these points and the horizontal. This angle is then compared to the angle for the second plane to give the total torsion. Such measurements in vitro have shown high precision and accuracy, with some authors claiming that little error is introduced when the long axis of the bone is deviated from the *Z*-axis of the dataset by up to 15° (Dähnert and Bernd

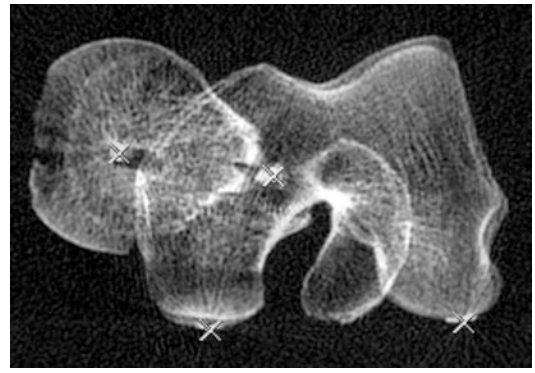

Fig. 2.5 Overlaid image of the axial sections that contain metal markers on the femoral head, neck and condyles. Planes between the relevant pairs of markers can now be drawn and the angle between them measured

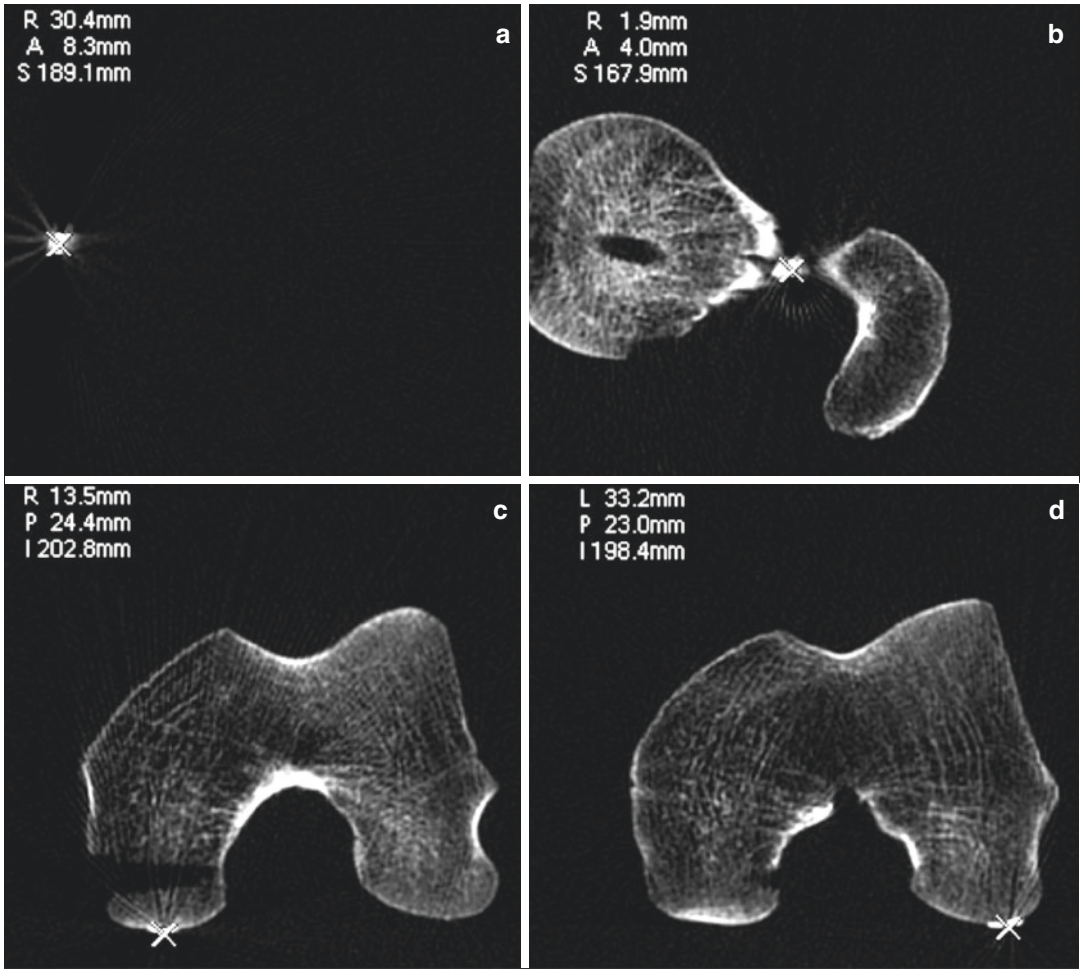

Fig. 2.6 (**a**–**d**) Axial sections through the metal markers on the femoral head (**a**), neck (**b**), medial (**c**) and lateral (**d**) posterior condylar surfaces. For each section, the scanner has identified the point location by reference to the scanner baseline isocentre, in millimetres to the right, left, anterior, posterior, superior or inferior. These relative locations in space allow geometric calculation of the planes, distances and angles between them. These same images are superimposed in Fig. 2.5

1986). Results of such measurements will, however, vary with the definition of the anatomical points used and may be influenced by flexion or varus deformity of the bone (Starker et al. 1998).

One study of femoral anteversion, using three-dimensional surface reconstructions of the femur from full CT image datasets, found them to be less reproducible than selected slice techniques when the femoral alignment was abnormal (flexed, adducted and internally rotated to simulate cerebral palsy), though the three-dimensional technique was more accurate (14% of measurements falling within 5° of actual, compared with 3% of 2D measurements) (Davids et al. 2003).

Three-dimensional surface reconstructions from MDCT data give a clear visual representation of the structure being assessed and make it easier to identify and correct for abnormal positioning. This is relevant, for example, in assessment of acetabular retro- or anteversion, where the measurement is influenced by pelvic tilting. Using 3D bone surface reconstruction of the pelvis, the pelvic tilt can be identified and the image rotated to correct it, with subsequent measurements of acetabular version being made in the true pelvic axial plane (Dandachli et al. 2009). The standardised pelvic plane joins the anterior superior ischial spines and the pubic tubercles (Fig. 2.7a), with the axial plane being perpendicular to this (Fig. 2.7b, c). Radiation dose reduction could be achieved by identifying the ASIS locations from limited low-dose sections through this level, rather than scanning the entire pelvis.

Assessment of the shape of the femoral head and neck is also currently in vogue, for the demonstration of bony deformities that cause cam impingement. Simple measurements of the alpha angle are influenced by the orientation of the plane of section chosen through the femoral head and neck. Using a MDCT 3D reconstruction of the proximal femur allows a full assessment of the location, size and "true" alpha angle of a cam deformity to be measured (Beaulé et al. 2005; Audenaert et al. 2011).

Three-dimensional surface reconstructions of the hips can also be used to identify the acetabular margin over the femoral head, to estimate femoral head coverage in dysplasia (Dandachli et al. 2008).

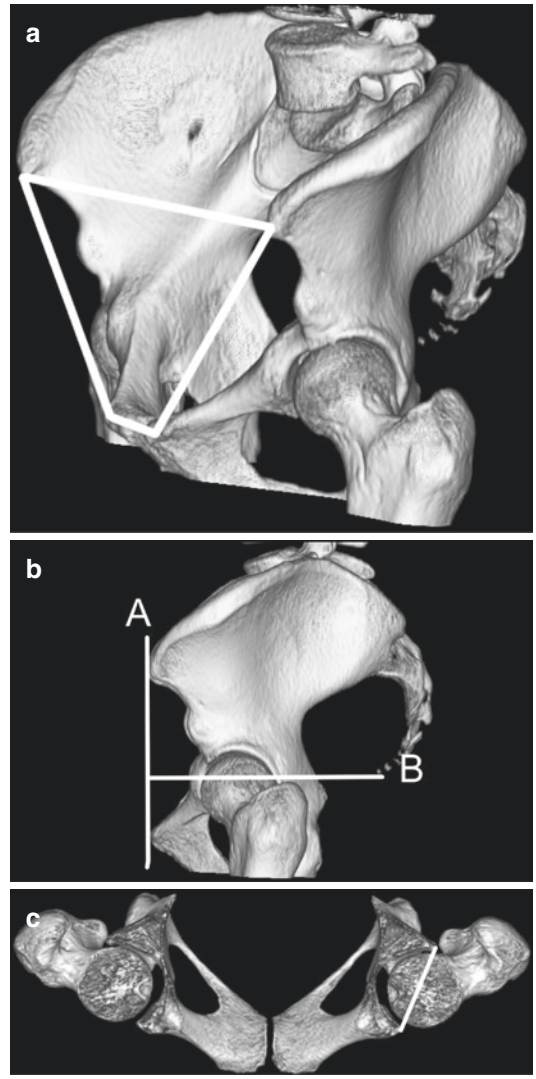

Fig. 2.7 (**a**) Automated 3D surface reconstruction of the pelvis from MDCT dataset. The white lines join the anterior superior iliac spines and pubic tubercles. (**b**) The image is then rotated until the plane defined by these lines is vertical (line "A") to correct pelvic tilt, the true axial plane (line "B") is perpendicular to this. (**c**) Axial plane measurements, (such as acetabular version) are then made in the true transaxial plane

Three-dimensional surface reconstructions of malunited fractures can also be manipulated on a workstation, with virtual correction of the deformity used to make custom jigs that fit onto the bone during surgery to identify the optimum osteotomy location and then fits the cut ends of the bone to allow accurate correction of the deformity (Murase et al. 2008).

Comparisons with Other Techniques (Linear Measurements)

Femoral anteversion has been measured clinically and by using plain radiography, CT, MR and ultrasound (Günther et al. 1996). CT is currently accepted as the standard for this measurement but has the limitation of a relatively high ionising radiation dose. Ultrasound measurement identifies surface locations on the bone; consequently, the absolute results obtained may differ from CT (Miller et al. 1993), where measurement points may be intra-osseous. Relative imprecision of ultrasound localisation of measurement points has been described, both as acceptable (Günther et al. 1996; Aamodt et al. 1995) and unacceptable in an earlier study using a static ultrasound scanner (Berman et al. 1987), for this measurement method. MR can achieve results similar to CT (Günther et al. 1996) and has the advantage of not using ionising radiation. This may therefore become the standard, particularly for measurement in children.

2.5 CT Volume Measurements

The approximate volume of structures with spherical or near spherical shapes can be estimated from measurement of the diameter of the structure in three orthogonal planes, averaging the result and calculating a volume using the formula for a sphere:

$$\text{Volume} = 4/3\pi\left(d/2\right)^3$$

π = pi
d = diameter

For irregular-shaped structures, where the boundaries are clearly defined by a steep CT number gradient (such as pulmonary nodules), then image analysis software packages are now available that will identify the lesion boundaries and calculate its volume automatically, from a summation of the contained pixel numbers and the voxel volume represented by each pixel. Similar manual methods have been used for decades, tracing the outline of the structure on each section, summating the areas obtained and multiplying by the slice spacing. Such manual methods have errors introduced by the window level, size and shape of the structure being measured and the surrounding tissue contrast (Schultz and Lackner 1980). The ratio of the *Z*-axis diameter of the structure being measured to the section thickness of the measurement slices will also influence volume estimation, in part due to partial volume averaging effects (Schultz and Felix 1978). Using low-dose 3-mm-thick sections applied to the orbits, resulting in on average ten contiguous sections through the structure of interest, we have achieved inter-observer precision of 1.3% and accuracy error of 1.5% for volume measurement (McGurk et al. 1992). Such methods have been applied to muscle volume measurement, for example, in the paraspinal muscles (Fig. 2.8) (Keller et al. 2003) and thighs (Rådegran and Saltin 2000). Measurement of fat and lean soft tissue areas can also be used to estimate body composition (Müller et al. 2002). In vivo measurements in animals (sheep) using just two sections through the hip and loin gave a correlation with dissection adipose mass of 0.79 (Lambe et al. 2006).

Estimation of lung volume from 3D MDCT volume reconstructions has been used to assess the impact of spinal scoliosis surgery (Gollogly et al. 2004a, b), with the degree of scoliosis also quantified three dimensionally (Dubousset et al. 2003). With the thin axial sections routinely produced by MDCT, high-resolution 3D images can be constructed with commercially available software, and the enclosed volume represented by the image (Fig. 2.9) can be automatically calculated.

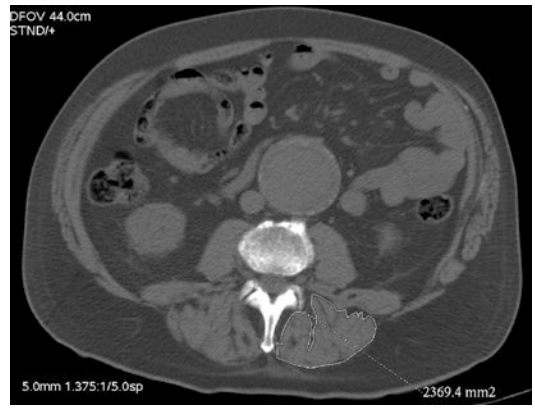

Fig. 2.8 Axial CT section through the mid-abdomen. A region of interest has been drawn around the left paraspinal musculature and its cross-sectional area measured

Fig. 2.9 Automated 3D reconstruction of the lungs from MDCT dataset. Commercially available software can measure the lung volume using similar image segmentation

As the lung/soft tissue and the bone/soft tissue interfaces are both high-contrast boundaries, a low-dose CT technique would be appropriate for this.

Semiautomated methods of lymph node volume and linear dimension measurements from MDCT data have been shown to be more precise and better predictors of disease involvement in lymphoma than manual measurements (Buerke et al. 2010).

2.6 CT Number Measurements

The CT number of a pixel in a CT image is an approximation to the Hounsfield value but requires calibration against a reference material to give an accurate Hounsfield unit measurement from an individual scan, as scanner calibration may drift with time and room temperature and may also vary with patient size. The Hounsfield value is a measure of the average voxel X-ray attenuation, compared to the attenuation of water, according to the formula:

$$HU_{(s)} = \left(\mu_{(s)} - \mu_{(w)} / \mu_{(w)}\right) \times 1000$$

$HU_{(s)}$ = Hounsfield unit value of substance filling the voxel

$\mu_{(s)}$ = linear attenuation coefficient of substance filling the voxel

$\mu_{(w)}$ = linear attenuation coefficient of water

Although this appears to calibrate Hounsfield unit measurements against water, the linear attenuation coefficients of different materials vary with X-ray photon energy. Consequently, the HU value of materials with higher average atomic numbers than water increase with reducing X-ray energy, and vice versa. Consequently, to use Hounsfield measurements to estimate the concentration or density of a known material, the scan is calibrated against that material, or an equivalent material of similar average atomic number.

Calibration against material within the patient can have limited application. Hepatic haemangiomas largely contain blood and consequently have CT numbers close to that of the patients' aorta (Whitehouse 1991).

Single Energy Quantitative Computed Tomography (SEQCT)

This technique is most often used to estimate vertebral trabecular bone mineral density. The patient is scanned whilst lying on a reference phantom which contains a water, or water equivalent, reference material and usually several different known concentrations of a bone mineral equivalent material, dissolved or suspended within water equivalent materials. A calibration curve of CT number against mineral concentration is produced from the reference materials, from which the CT number of a region of interest in the vertebral trabecular bone can be converted into a mineral density equivalent. With care and experience, measurements with a precision error (reproducibility) of better than 1% can be achieved.

Dual-Energy Quantitative Computed Tomography

SEQCT is precise but lacks accuracy, as (for vertebral mineral densitometry) the presence of variable amounts of marrow fat cannot be accommodated for. The linear attenuation coefficients for the three materials in a vertebra (bone, red marrow and yellow marrow) are widely different and also change in different directions with changing scanner kVp. Theoretically, scanning the vertebra at two different kVp values can be used to estimate the proportions of each by solving the simultaneous equations below:

$$V_b + V_r + V_y = 1.$$

$$HU_b(l) \times V_b + HU_r(l) \times V_r + HU_y(l) \times V_y = HU_v(1).$$

$$HU_b(h) \times V_b + HU_r(h) \times V_r + HU_y(h) \times V_y = HU_v(h).$$

where

V_b, V_r and V_y are the volume proportions of bone, red marrow and yellow marrow, respectively.

$HU_b(l)$, $HU_r(l)$, $HU_y(l)$ and $HU_v(l)$ are the Hounsfield unit values for bone, red marrow, yellow marrow and the vertebral region of interest at the low kVp scan.

$HU_b(h)$, $HU_r(h)$, $HU_y(h)$ and $HU_v(h)$ are the Hounsfield unit values for bone, red marrow, yellow marrow and the vertebral region of interest at the high kVp scan.

HU_b, HU_r and HU_y are measured from materials in the reference phantom, and HU_v is measured in the vertebra, at each scan energy, respectively. V_b, V_r and V_y are the unknowns.

Reference materials for red and yellow marrow (and even bone) are somewhat unsatisfactory. Large errors can occur if the materials do not show the same X-ray energy-dependent change in attenuation as the material being measured. A sophisticated method of overcoming this limitation of reference material was described by Nickoloff, who used the reference phantom calibration curve to estimate the effective X-ray energy of the scan and then used published linear attenuation coefficient data to calculate the expected Hounsfield unit values of the materials, rather than measuring them from a phantom (Nickoloff et al. 1988).

Dual-energy QCT has not been widely used, as it increases the patient radiation dose, is in practice of little advantage over SEQCT and has a considerable poorer precision. The error in SEQCT bone mineral estimation attributable to marrow fat is in the range of 5–15% and has a significant age dependency. Consequently, if age-related reference data is used, the error is relatively small (Glüer and Genant 1989). A further improvement in the accuracy of SEQCT for bone mineral estimation is achieved by lowering the kVp, on those scanners with this facility. At 80 kVp (instead of the more usual 120–140 kVp), the CT number for mineral is markedly increased, whilst the reduction in CT number for fat is less great. Consequently, the CT number for a mixture of the two has a greater dependence upon the mineral concentration. DEQCT has been used to estimate liver iron in patients with haemochromatosis and haemosiderosis from repeated transfusion. There may be a recrudescence of interest with the development of a dual X-ray source CT scanner that acquires both energies almost simultaneously and can produce separate high and low atomic number material images directly.

Comparisons with Other Measurements (Density Measurements)

Currently, the accepted standard technique for bone mineral density measurement is dual-energy X-ray absorptiometry (DXA). This method utilises low-dose X-rays, filtered to produce alternating high- and low-energy X-ray beams and scanned across the region of interest. Results of these scans give an estimate of the total mineral in the scan path, per unit area of the projection; thus trabecular and cortical bone (plus any soft tissue calcification, facet joint osteoarthosis) that lies in the same part of the projected image is included in the result. Despite these limitations, DXA is a very precise measurement method; uses lower X-ray doses than QCT; can provide measurements in the spine, hip, whole body or selected regions; and is cheaper. Consequently, it was adopted by the WHO within its definition of osteoporosis (Miller 2006). QCT has the advantage of measuring trabecular bone separately from cortex and other calcifications and being a true volumetric density is not influenced by patient size.

Conclusions

Computed tomography produces images of excellent dimensional stability. When submillimetre section thickness is used, clearly defined anatomical points can be located in all three dimensions and measurements between them made with high accuracy. The limitation, as with all measurement, is largely in the anatomical definition and precision of point placement. Care to ensure that slice location is correct, that the patient does not move between slice acquisitions and that appropriate consideration of the three-dimensional geometry is allowed for in the measurement technique should optimise the result. Steps to minimise X-ray dose to the patient should be routinely employed—low mA, low kV scans and the use of low mA scout views to place the minimum number of axial sections required for the measurement. Lead gonad protection can also be used for the scout views and high-density (bismuth) protectors can also reduce radiation dose to selected superficial structures on axial sections, without significantly impairing image quality (Hohl et al. 2006).

References

Aamodt A, Terjesen T, Eine J, Kvistad KA (1995) Femoral anteversion measured by ultrasound and CT: a comparative study. Skelet Radiol 24:105–109

Audenaert EA, Baelde N, Huysse W, Vigneron L, Pattyn C (2011) Development of a three-dimensional detection method of cam deformities in femoroacetabular impingement. Skelet Radiol 40:921–927

Beaulé PE, Zaragoza E, Motamedi K, Copelan N, Dorey FJ (2005) Three-dimensional computed tomography of the hip in the assessment of femoroacetabular impingement. J Orthop Res 23:1286–1292

Berman L, Mitchell R, Katz D (1987) Ultrasound assessment of femoral anteversion. A comparison with computerised tomography. J Bone Joint Surg Br 69:268–270

Buerke B, Puesken M, Müter S, Weckesser M, Gerss J, Heindel W, Wessling J (2010) Measurement accuracy and reproducibility of semiautomated metric and volumetric lymph node analysis in MDCT. Am J Roentgenol 195:979–985

Dähnert W, Bernd W (1986) Computertomographische Bestimmung des Torsionswinkels am Humerus. Z Orthop Ihre Grenzgeb 124:46–49

Dandachli W, Kanna V, Richards R, Shah Z, Hall-Craggs M, Witt J (2008) Analysis of cover of the femoral head in normal and dysplastic hips: new CT-based technique. J Bone Joint Surg Br 90-11:1428–1434

Dandachli W, Ul Islam S, Liu M, Richards R, Hall-Craggs M, Witt J (2009) Three-dimensional CT analysis to determine acetabular retroversion and the implications for the management of femoro-acetabular impingement. J Bone Joint Surg Br 91-8:1031–1036

Davids JR, Marshall AD, Blocker ER, Frick SL, Blackhurst DW, Skewes E (2003) Femoral anteversion in children with cerebral palsy. Assessment with two and three-dimensional computed tomography scans. J Bone Joint Surg Am 85-A:481–488

Dubousset J, Wicart P, Pomero V, Barois A, Estournet B (2003) Spinal penetration index: new three-dimensional quantified reference for lordoscoliosis and other spinal deformities. J Orthop Sci 8:41–49

Glüer CC, Genant HK (1989) Impact of marrow fat on accuracy of quantitative CT. J Comput Assist Tomogr 13:1023–1035

Gollogly S, Smith JT, Campbell RM (2004a) Determining lung volume with three dimensional reconstructions of CT scan data. A pilot study to evaluate the effects of expansion thoracoplasty on children with severe spinal deformities. J Pediatr Orthop 24:323–328

Gollogly S, Smith JT, White SK, Firth S, White K (2004b) The volume of lung parenchyma as a function of age: a review of 1050 normal CT scans of the chest with three-dimensional volumetric reconstruction of the pulmonary system. Spine 29:2061–2066

Günther KP, Kessler S, Tomczak R, Pfeifer P, Puhl W (1996) (femoral anteversion: significance of clinical methods and imaging techniques in the diagnosis in children and adolescents). Title in original lang. Femorale Antetorsion: Stellenwert klinischer und bildgebender Untersuchungsverfahren bei Kindern und Jugendlichen. Z Orthop Ihre Grenzgeb 134:295–301

Hohl C, Wildberger JE, Süss C, Thomas C, Mühlenbruch G, Schmidt T, Honnef D, Günther RW, Mahnken AH (2006) Radiation dose reduction to breast and thyroid during MDCT: effectiveness of an in-plane bismuth shield. Acta Radiol 47:562–567

Keller A, Gunderson R, Reikerås O, Brox JI (2003) Reliability of computed tomography measurements of paraspinal muscle cross-sectional area and density in patients with chronic low back pain. Spine 28:1455–1460

Lambe NR, Conington J, McLean KA, Navajas EA, Fisher AV, Bünger L (2006) In vivo prediction of internal fat weight in Scottish blackface lambs, using computer tomography. J Anim Breed Genet 123:105–113

McGurk M, Whitehouse RW, Taylor PM, Swinson B (1992) Orbital volume measured by a low-dose CT scanning technique. Dentomaxillofac Radiol 21:70–72

Miller PD (2006) Guidelines for the diagnosis of osteoporosis**:** T-scores vs fractures. Rev Endocr Metab Disord 7:75–89

Miller F, Merlo M, Liang Y, Kupcha P, Jamison J, Harcke HT (1993) Femoral version and neck shaft angle. J Pediatr Orthop 13:382–388

Müller MJ, Bosy-Westphal A, Kutzner D, Heller M (2002) Metabolically active components of fat-free mass and resting energy expenditure in humans: recent lessons from imaging technologies. Obes Rev 3:113–122

Murase T, Oka K, Moritomo H, Goto A, Yoshikawa H, Sugamoto K (2008) Three-dimensional corrective osteotomy of malunited fractures of the upper extremity with use of a computer simulation system. J Bone Joint Surg Am 90-A:2375–2389

Nickoloff EL, Feldman F, Atherton JV (1988) Bone mineral assessment: new dual energy approach. Radiology 168:223–228

Rådegran G, Saltin B (2000) Human femoral artery diameter in relation to knee extensor muscle mass, peak blood flow, and oxygen uptake. Am J Physiol Heart Circ Physiol 278:H162–H167

Schultz E, Felix R (1978) Phantommessungen zum räumlichen Auflösungsvermögen und zum Partial-Volume-Effect bei der Computertomographie. Rofo 129:673–678

Schultz E, Lackner K (1980) Die Bestimmung des Volumens von Organen mit der Computertomographie. I. Die Ermittlung von Organquerschnittsflächen unter Berücksichtigung der dabei auftretenden Fehlermöglichkeiten. Rofo 132:672–675

Starker M, Hanusek S, Rittmeister M, Thoma W (1998) Validierung computertomographisch gemessener Antetorisonswinkel am Femur. Z Orthop Ihre Grenzgeb 136:420–427

Togashi K, Kitaura H, Yonetsu K, Yoshida N, Nakamura T (2002) Three-dimensional cephalometry using helical computer tomography: measurement error caused by head inclination. Angle Orthod 72:513–520

Whitehouse RW (1991) Computed tomography attenuation measurements for the characterization of hepatic haemangiomas. Br J Radiol 64:1019–1022

Ultrasound

3

Carlo Martinoli, Ali Attieh, and Alberto Tagliafico

Contents

3.1 Introduction

Measurement is one of the key parameters of US examination and represents an essential part for a correct interpretation of ultrasound (US) images and for distinguishing normal from pathologic conditions. In the musculoskeletal system, US measurements involve calculation of linear distance, area, or volume. Distance measures are the most commonly used by far. They are usually obtained on the freezed image frame by moving a visible cursor on the screen via a track ball: the process may take a couple of seconds. The precision of distance measurements reached by current technology and high frequency broadband transducers is very high, and, in the best circumstances, spot reflectors measuring 0.1 mm in size can be resolved as separate structures. Area measurements are used in more specific settings. Because most of area measurements relate to round/oval structures, built-in systems that produce an ellipse on the screen can give results quickly by adjusting size and shape on the structure to be evaluated with the track ball. On the other hand, freehand area measurements need a steady hand: it may be difficult to draw on the screen a trace that perfectly overlaps the structure of interest. However, positive and negative errors produced by the caliper spots that deviate from the intended position on either side of the outline, at the end, tend to balance. Automated recognition algorithms have recently been introduced to

C. Martinoli, M.D. (✉) • A. Attieh, M.D.
A. Tagliafico, M.D.
Radiologia— Department of Health Science, Università di Genova, Ospedale Policlinico San Martino, Genova, Italy
e-mail: carlo.martinoli@libero.it

V. N. Cassar-Pullicino, A. M. Davies (eds.), *Measurements in Musculoskeletal Radiology*, Medical Radiology, Diagnostic Imaging, https://doi.org/10.1007/978-3-540-68897-6_3

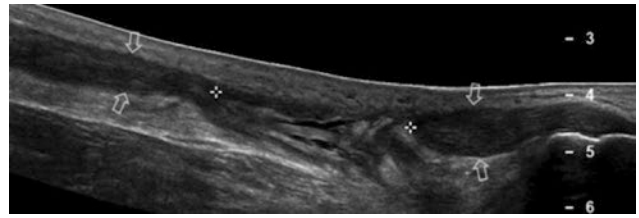

Fig. 3.1 Longitudinal extended field-of-view 12–5 MHz US image of the posterior ankle in a patient with chronic Achilles tendon rupture and substantial retraction of the tendon ends (*arrows*). The length of the gap exceeds the transducer width but can be effectively measured by means of the extended field-of-view technique

make precise tracing around a given structure without wasting time. If implemented in the equipment software, volume algorithms usually refer to ellipsoid structures or recall obstetrical shapes. In general, these systems do not perfectly fit for use in the musculoskeletal system, where skeletal muscles have variable conformation. The advent of 3D and 4D ultrasound is opening new perspectives in this field. One of the main drawbacks of linear array transducers is the limited extension of the field of view that makes measurements of elongated structures in the musculoskeletal system impractical. Thus, spatial relationships and sizes in the US images often must be synthesized in the mind of the sonologist from multiple real-time images that display only portions of the relevant anatomy (Lin et al. 1999). With extended field-of-view systems, however, geometric measurements can be obtained effectively from lesions larger than the field of view of the transducer with <5% error (Fig. 3.1) (Fornage et al. 2000).

The aim of this chapter is to discuss technical aspects of US measurement of tendons, muscles, nerves, joints, and soft-tissue masses and to determine under what circumstances these measurements are used in the musculoskeletal system.

3.2 Tendons

One of the most common applications of musculoskeletal US is the investigation of tendons (Martinoli et al. 1999, 2002). Nevertheless, limited data are available in literature regarding reproducibility of tendon measurements and observer variability in obtaining these measures (Ying et al. 2003; O'Connor et al. 2004). This may be in part related to intrinsic factors, such as the existence of wide range variation of tendon size depending on gender, side dominance, and effects of sports exercise (Koivunen-Niemelä and Parkkola 1995; Ying et al. 2003). On the other hand, technical factors, including lack of adequate standardization of probe positioning, differences in pressure applied with the probe and angles of incidence of the US beam as well as absence of clearly defined landmarks around tendons, contribute to make difficult obtaining comparable images and reproducible measurements. Based on recent studies, interobserver variation was found to be a greater source of error than intraobserver variation when measuring tendons (O'Connor et al. 2004). In general terms, this would support the use of the same observer if longitudinal studies of tendon size have to be undertaken.

3.3 Tendinosis and Partial Tears

The degenerative process in tendons, which is commonly known as "tendinosis," has imaging characteristics that may be used alone or in combination to help in distinguishing this process from normal states or other more severe tendon abnormalities such as complete tears. Among them, an increased size of the affected tendon in the zone of abnormality is virtually pathognomonic of the degenerative process that produces an increase in the glycoprotein matrix, tenocyte, and fibroblast proliferation with the formation of disorganized collagen (Martinoli et al. 2002). Measurement of thickness and determination of increased size is thus an important component of tendon assessment, reflecting both status and severity of tendinopathy (Archambault et al. 1998). In the degenerative setting, the abnormal tendon may thicken circumferentially, leading to a parallel increase in size of the two axial diameters (AP and LL) or may enlarge selectively along the surface-to-depth axis (AP). This "vertical" swelling most often occurs close to bone insertions (e.g., lateral epicondylitis, jumper's knee, etc.). As a rule, it would be, therefore, recommended to calculate the tendon size in the zone of maximum thickening by considering the cross-sectional area (given by calculation of the two axial diameters or by tracing methods provided by the built-in software of the equipment). In alternative, the examiner should take the only AP diameter, which is expression of the tendon thickness. When measuring this parameter, the screen calipers should be placed systematically on the short axis of the tendon to obtain more reliable calculation, because the longitudinal plane may overestimate the tendon thickness due to partial volume averaging artifact and some obliquity in the course of tendons (Fig. 3.2) (Fornage 1986; Ying et al. 2003). If the increased tendon volume is mild (grade I tendinopathy), it may be recognized in a more confident way by comparing the affected tendon with the contralateral one (if this latter is healthy). In tendinosis, measurement accuracy would have potential implications not only to identify mild disorder but also to follow-up tendon changes and evaluate the effects of conservative measures with time. On the other hand, high values of tendon thickness have also been proposed to correctly predict tendinosis and partial tears, at least in the Achilles tendon (Hartgerink et al. 2001). Softening (tenomalacia) is another feature of tendons affected by degenerative changes and partial tears (Koury and Cardinal 2009). Under certain circumstances, probe compression may be useful in distinguishing between effusion and synovial hypertrophy filling a partial-thickness tear (soft) from residual intact tendon fibers (stiff). In the absence of a tear, an increased tendon compressibility may be encountered in abnormally thickened tendons as a result of deranged intratendinous structure (Koury and Cardinal 2009). Compressibility can be visually assessed on gray-scale imaging applying graded compression with the probe on the abnormal tendon. This evaluation should be performed in a relaxed state, without applying any tension to the tendon fibers. More recently, sonoelastography, a relatively new technique that is able to assess the elastic properties of tissues, can offer better quantitative analysis of tendon compressibility (strain) expressed in pressure units, commonly kilopascals (kPa), or as a strain ratio (Klauser et al. 2010). Initial application of sonoelastography in lateral epicondylitis and Achilles tendinopathies showed promising results (De Zordo et al. 2009, 2010; Drakonaki et al. 2009). In most cases, however, this modality should be viewed as emerging rather than an established tool of assessment. A standardized protocol for image acquisition, range of values, and limitations need to be defined in this setting. Further clinical evaluation is also mandatory.

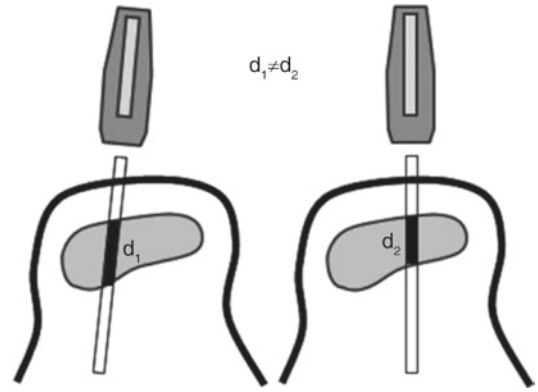

Fig. 3.2 Tendon thickness measurement. Schematic drawings illustrate possible sources of inaccuracy when placing the probe over the long axis of the tendon. Slight tilting of the probe or some obliquity of the tendon relative to the skin may cause calculation errors of tendon diameter (*d*) and poor reliability